TYCO LABORATORIES, INC., BEAR HILL, WALTHAM, MASSACHUSETTS 02154 TELEPHONE 617 899-1650

Development of Continuous, High Efficiency, Room Temperature, Visible Wavelength, Semiconductor Injector Lasers

FINAL REPORT

Contract No. NAS8-11864

For
National Aeronautics and Space Administration
George C. Marshall Space Flight Cen
Huntsville, Alabama

Tyco Laboratories, Inc.
Bear Hill
Waltham, Massachusetts

DEVELOPMENT OF CONTINUOUS, HIGH EFFICIENCY, ROOM TEMPERATURE, VISIBLE WAVELENGTH, SEMICONDUCTOR INJECTOR LASERS

FINAL REPORT

Contract No. NAS8-11864

For

National Aeronautics and Space
Administration
George C. Marshall Space Flight Center
Huntsville, Alabama

CONTENTS

I. INTRODUCTION

This is the final report under Contract NAS8-11864 of which the principal objective was the development of a semiconductor injection laser to operate continuously at room temperature in the visible wavelength range. This wavelength requirement limits the choice of semiconductors to very few, of which GaP and SiC are held to be the only promising candidates. Under this program α-SiC has been investigated, since earlier work at the laboratory indicated laser action from p-n junction diodes of α-SiC prepared by growth from chromium solution.

Because of inherent difficulties in achieving reproducibility in the physical and chemical properties of SiC, we have been unsuccessful in our attempts to repeat the earlier results. However, a great deal has been learned about the electro-optical properties of SiC and also considerable progress has been made in terms of device technology and evaluation procedures.

Probably one of the most significant scientific findings to evolve from this program is that the electroluminescent spectrum of α-SiC can be quite markedly affected by specific impurities (not dopants in the usual sense). It has been shown that specific levels (presumably quite deep) introduced by transition elements can be pumped electrically, and the efficiency of the recombination process appears to be dependent upon the particular impurity. While these findings are of interest themselves in terms of an understanding of large band gap, indirect semiconductors, we are now of the opinion that our earlier findings of what we believe to have been laser action are intimately connected with a set of specific impurity levels. Those factors discussed in our Proposal, namely junction abruptness and defect structure, have been reproduced. It would therefore appear

that while these are probably necessary, they are by no means sufficient conditions. Therefore, because of the many interacting complications, this program has really been a materials study, but very much in the realm of solid state physics.

In the following pages we describe the principle accomplishments of the program. Section II describes the evaluation procedures which have been devised to study the diodes. Section III outlines the progress which has been made in device design and construction. (These procedures have, we feel, applicability to types of SiC devices other than those for optical use.) Section IV is a discussion of our experimental findings on the devices themselves, including the work on transition-element doping.

II. EVALUATION PROCEDURES

There are basically three areas where routine evaluation is required. Firstly, since the raw material (SiC crystal) is obtained from an outside source and is generally not characterized, it is necessary to determine conductivity type, resistivity, and crystalline defect density. Conductivity type is relatively straightforward in α-SiC, since pronounced color differences exist between p-type (blue) and n-type (green). In general we have, for obvious reasons, obtained material of the lowest possible resistivity. Determination is made using a contactless resistivity probe. In general, resistivities range from 0.01 - 1 Ω cm with n-type material yielding lower values than for p-type material. Cross checks have been made utilizing samples on which four alloyed contacts were made and employing the well known Van der Paue method. Determination of dislocation densities in as-received crystals has been made using etch pit techniques (etching solution: 3 parts NaOH + 1 part Na_2O_2

at 700°C). Pits are counted directly under the optical microscope.

These techniques are, of course, not new, and are mentioned herein for the sake of completeness only. However, the wide range of resistivities quoted above together with the data of etch pit densities presented in Table I illustrate one of the principle sources of the difficulties encountered with SiC. It is noteworthy that the crystals under discussion are typical of the best available.

TABLE I

Dislocation Density of α-SiC Crystals

Supplier's Lot Number	Conductivity Type	Average Etch Pit Count per cm^2
8897	P	2,700
8897	P	5,900
8897	P	1,577
8897	P	16,384
8897	P	9,728
8994	N	12,766
8994	N	96,128
8994	N	27,300
1-65	P	5,120
1-65	P	11,366
1-65	P	12,042
1-65	P	4,423
1-65	P	7,500
1-65	P	3,375
1-65	P	3,100
1-65	P	10,300

The second evaluation stage involves ohmic contacts. In the early stages of this program we examined various contacting procedures which were evaluated in terms of specific contact resistance and of linearity.

Contacts were made to single crystal slices of both p- and n-type material, and these were examined according to the above two properties. To facilitate the examination, an ac bridge was designed and constructed according to the circuit shown in Fig. 1. The operation of the bridge is quite simple, values being read directly from an oscilloscope trace. To determine the linearity (expressed as % non-linearity), the straight line portion is "nulled-out" and the remaining non-linear portion alone is displayed on the scope. As an arbitrary, but nevertheless realistic, standard, contacts of less than 1% non-linearity are considered "ohmic" while contacts of greater than 1% non-linearity are considered "non-ohmic". Using this procedure comparisons between the various contacting methods and also the temperature dependence of individual contacts have been made (the findings are presented in Section III).

The detailed evaluation of diodes has accounted for the majority of our efforts on this program. The evaluation methods may be divided into two areas:

(1) low current (diode) properties

(2) high current (electroluminescent) properties.

Paramount among the low current properties are the forward I-V characteristics, the diode resistance, and the junction capacitance.

From a measurement of the junction capacitance per unit area, an indication of the carrier concentration at the junction may

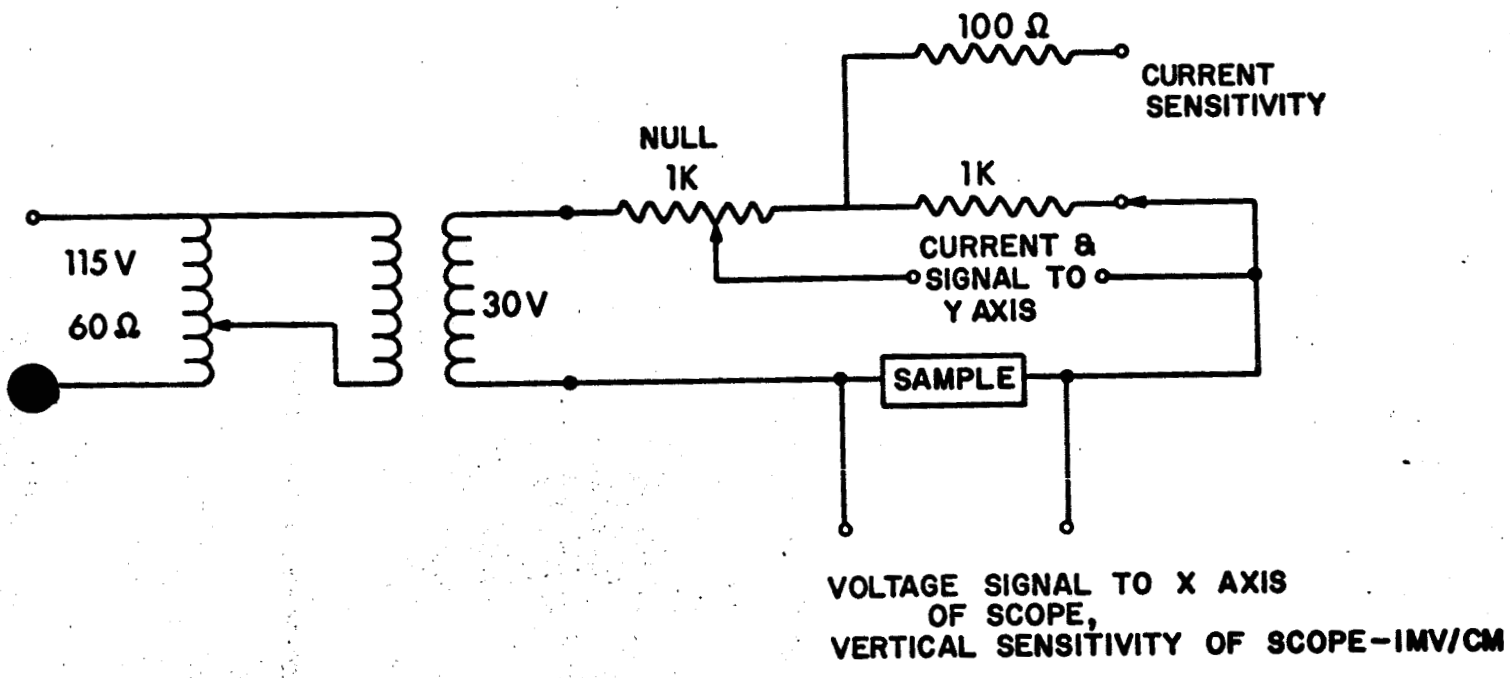

Fig. 1 A.c bridge for measurement of non-linearity of contacts.

be obtained. Expressing this as a figure of merit (FM), in units of picofarads per square mil, a master curve relating FM to junction carrier concentration may be developed. This is shown in Fig. 2. A value of unity for FM indicates a minimum carrier concentration of 10^{18} per cc.

The diode series resistance, R_s, is calculated from the measured conductance as $R_s = G/C^2$ x constant. This has proved to be a useful parameter since, when R_s is large ($>10\Omega$) and FM is greater than unity, poor contacts are indicated.

To facilitate rapid evaluation of the I-V characteristics, a logarithmic amplifier has been constructed, which produces an output of exactly one volt per decade over a range of currents from 5×10^{-10} amps to 10^{-1} amps. The conversion accuracy of the logarithmic unit is within $\pm 1\%$ over this entire range.

The unit is based upon the proposition that if the collector-base voltage of a transistor were held to be zero or a few tenths of V_o, where

$$V_o = \frac{kT}{9} \tag{1}$$

then the collector current is given by the expression

$$I_c = I_o \exp \left\{ V_{be}/V_o \right\} \tag{2}$$

where all quantities are positive for an npn transistor. This expression is valid for any transistor, whether or not the emitter-base or base-collector junctions obey individually ideal diode behavior.

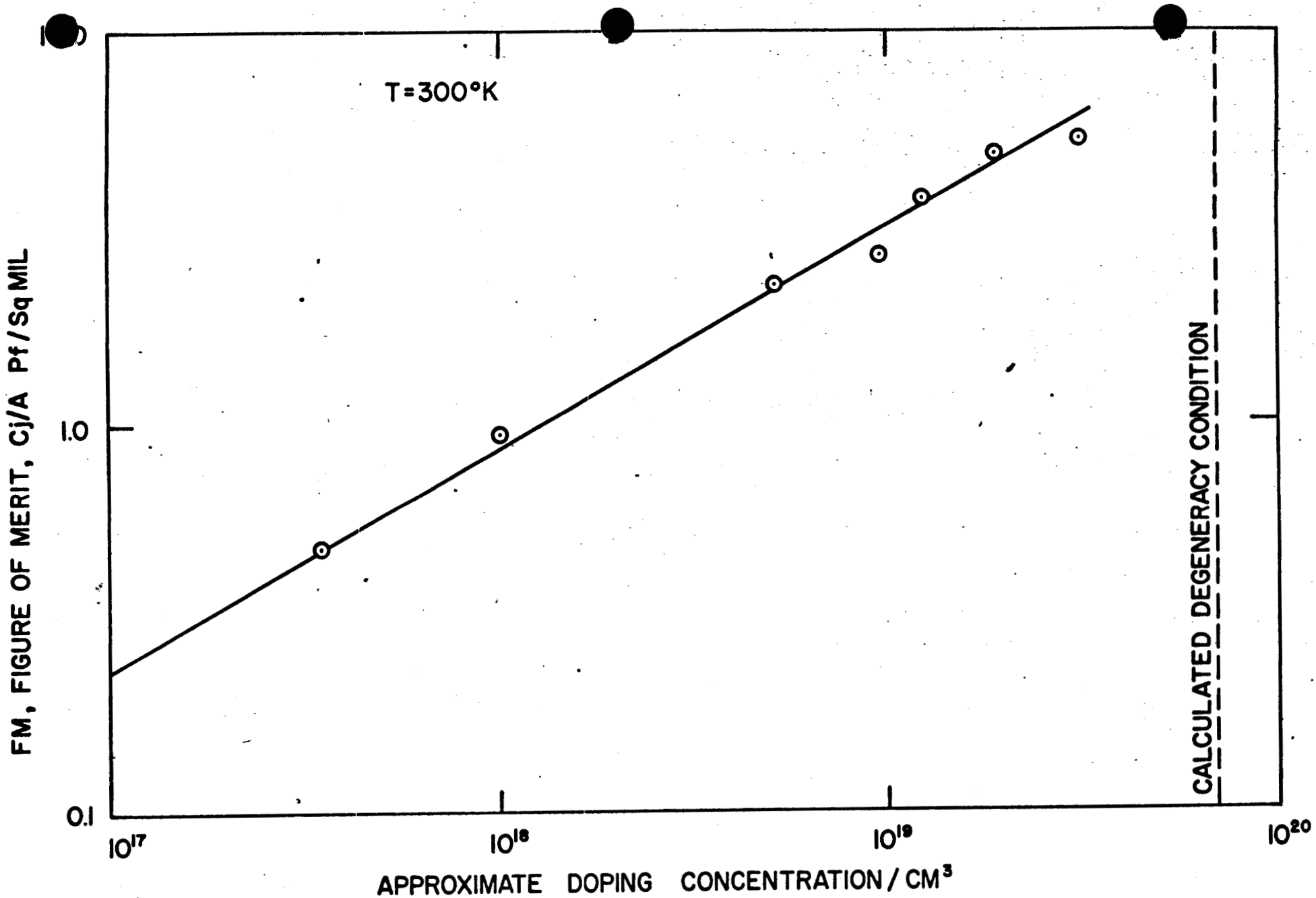

Fig. 2 Relationship of doping level and Figure of Merit observed on some TSM grown SiC diodes.

One means of satisfying the condition $V_{cb} \tilde{=} 0$ is to use an operational amplifier, Fig. 3. Neglecting the off-set current of the amplifier and its off-set voltage, the collector current will equal the input current, I, and the amplifier output voltage will be

$$E_a = E_o \log \frac{I_i}{I_o} \quad ; \quad E_o = 2.33\, V_o \tag{3}$$

A true logarithmic transfer is possible with Fig. 3 over the range 5×10^{-10} to 10^{-2} amps, assuming a perfect amplifier. The output voltage, however, will be unusable unless the temperature is held within $\pm .05^{o}C$, due to the extreme temperature sensitivity of the base collector saturation current, I_o. Since this degree of temperature control is difficult to achieve practically at moderate cost, a difference-amplifier technique has been devised. If another circuit like Fig. 3 with

$$E_b = E_o \log \frac{I_r}{I_o} \tag{4}$$

and using a transistor with the exact same I_o, mounted in isothermal relation to that of the transistor in Eq. (1) is connected to a difference-amplifier, then the output of the difference-amplifier, E_d, is

$$E_d = K(E_a - E_b) = K E_o \log \frac{I_i}{I_r} \tag{5}$$

and no longer contains the saturation current component. If the gain constant, K, is chosen to be 1000/59.6, then, at room temperature, a logarithmic output of exactly one volt per decade change in the input current, I, will result. This output will vary

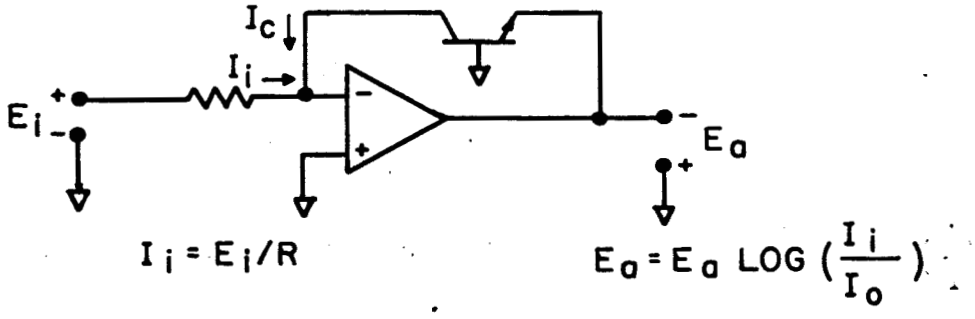

Fig. 3 Patterson diode connection for producing wide-range logarithmic signal conversion. Ref. 1.

approximately .3% per ^{o}C at room temperature.

Using commercially available amplifiers, it was found that a circuit could be assembled to work over the range from 5×10^{-10} amps to 10^{-3} amps. It was desired to extend the range to 10^{-1} amps without having to throw any switches manually. An automatic range extender circuit was devised, which divides the input current to the amplifier by 100 and adds 2 volts to the output once 8×10^{-2} amps is reached, and reverses this procedure once the current drops below 6×10^{-2} amps. This circuit was required to have approximately 2.2 volts hysteresis in it for stability. A Tyco-made silicon carbide diode and a silicon diode were combined in a parallel arrangement, Fig. 4, which has the characteristics of a 2.2 volt dead band, due to the 1.6 volt forward bias voltage drop of SiC and the .6 volt forward bias drop of the Si.

The complete log amplifier circuit is shown in Fig. 5.

In practice, SiC diodes are measured by application of a voltage ramp to the diode. The x-axis of an x-y recorder records this voltage, while the y-axis records the output of the log amplifier, the input of which is the diode current.

The principle high current measurements relate directly to the electroluminescent properties of the diodes. More specifically, this means the variation of optical efficiency with current density. The apparatus shown schematically in Fig. 6 has been used for this purpose.

A photomultiplier (RCA, type 5819) with maximum spectral response at 4500 Å was selected for the measurement of electroluminescent light output of α-SiC diodes. This tube has a cutoff to 50% sensitivity at 3500 Å and 5750 Å. This spectral range was considered adequate to study the light output of α-SiC diodes which

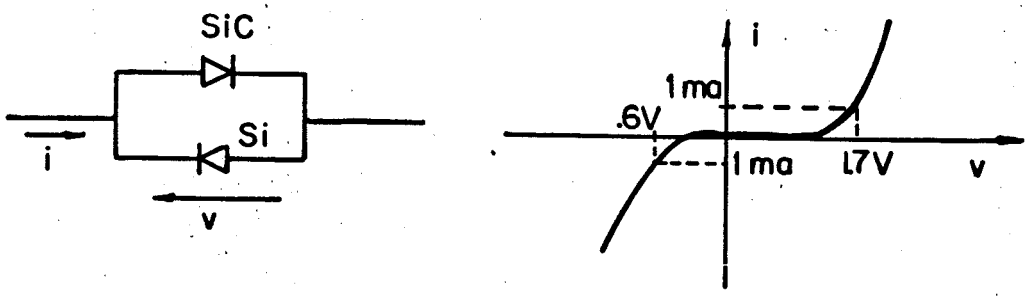

Fig. 4 Hysteresis backlash circuit using SiC and Si diodes.

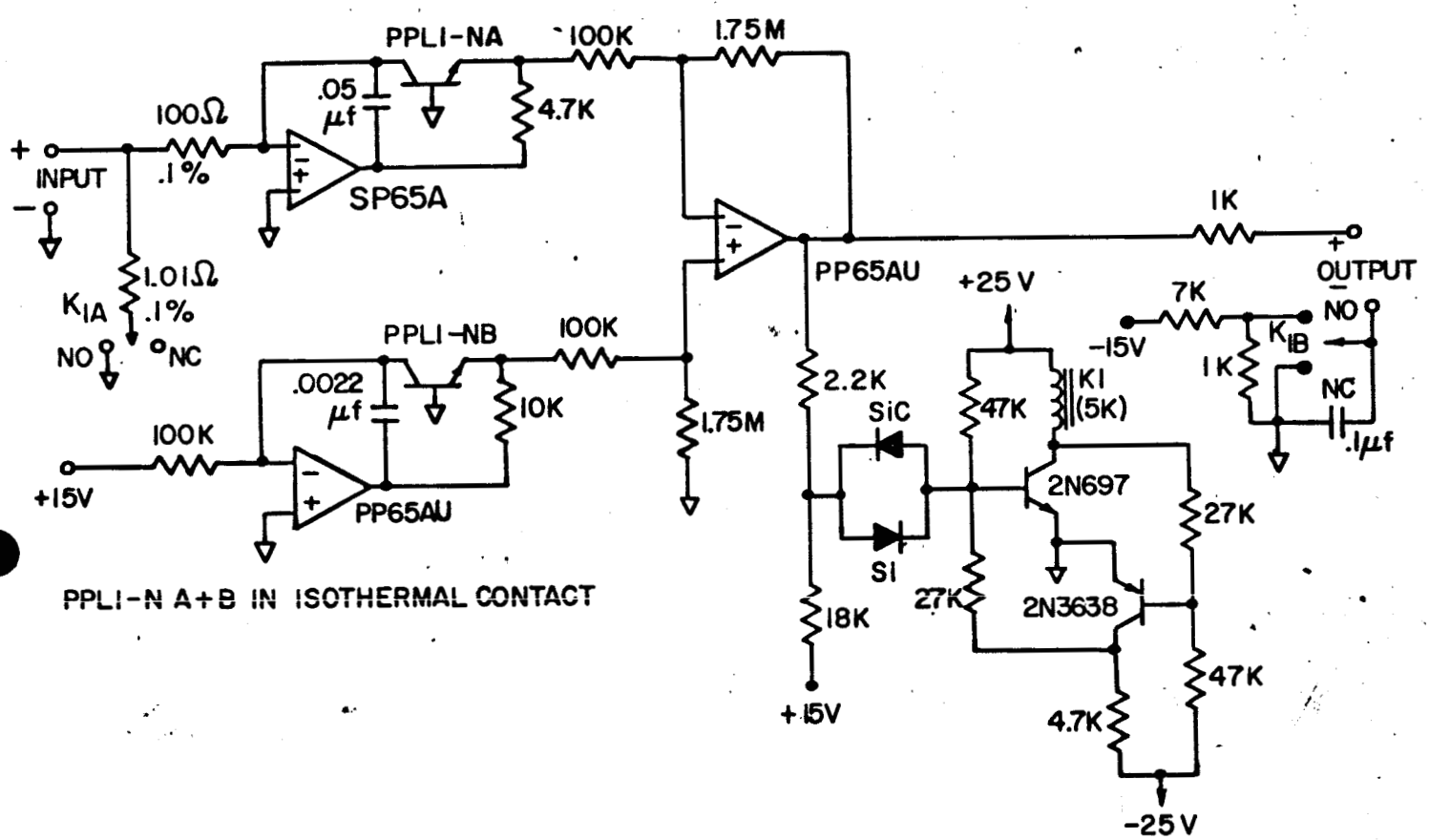

Fig. 5 Complete log-amp circuit. 5×10^{-10} amps to 10^{-1} amps. 1% conversion accuracy, 0.3% per ^{o}C conversion stability.

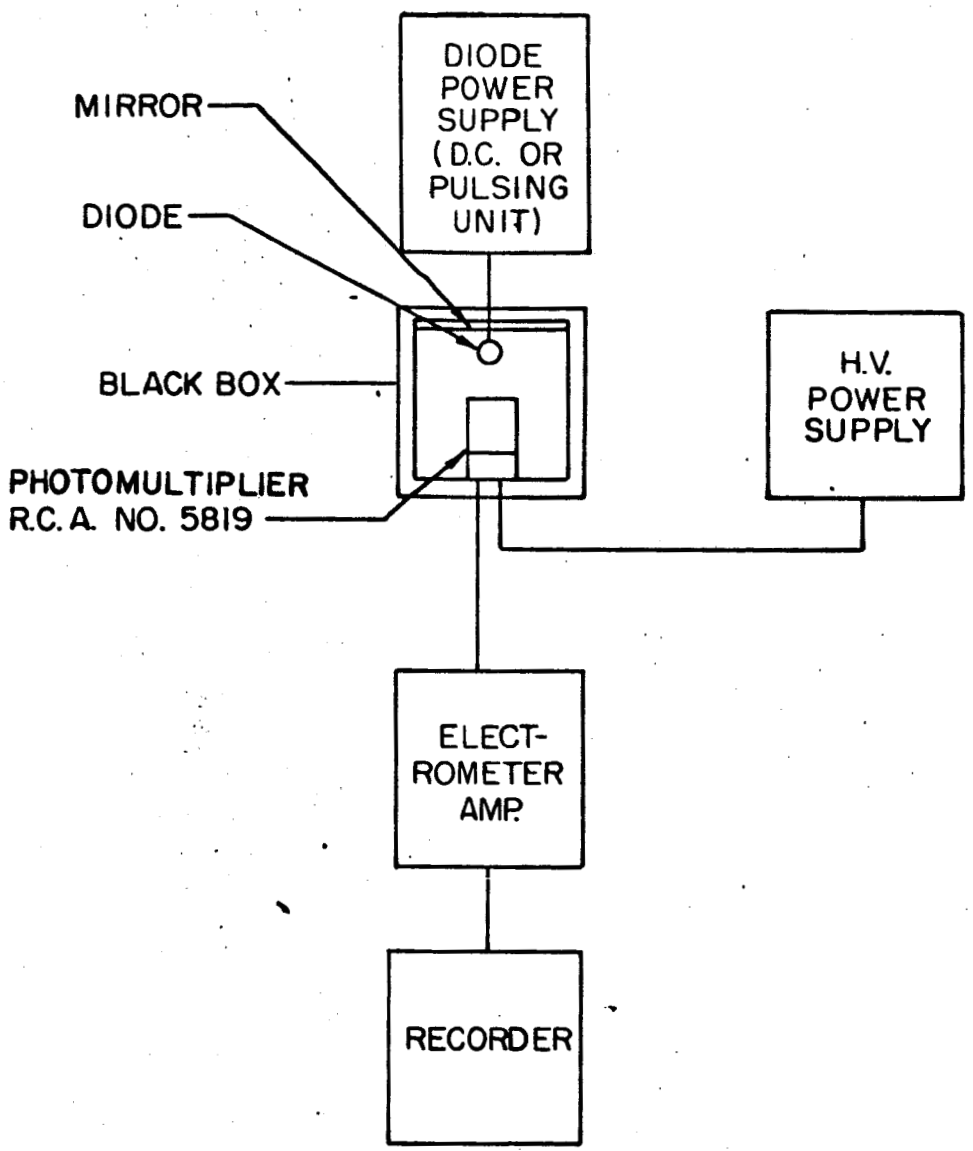

Fig. 6 Measurement of electroluminescence efficiency of SiC diodes.

exhibit peak spectral emission under 5500 Å. The diode under test is mounted upon a metal block which may be cooled by immersion in a liquid nitrogen placed beneath the "black-box". Adequate heat sinking of diodes has been obtained with this arrangement.

Using this setup the quantum and power efficiencies are quite readily determined. The photomultiplier is first calibrated with use of a standard light source. Determinations have been made both as a function of current density and of temperature.

Measurements of the spectral distribution of the light output from our diodes have been made using a Czerny-Turner 3/4 meter grating spectrometer. A simple modification has been made to the mechanical rotation (linearly proportional to wavelength) of the unit. By application of some electromechanical transducers, the mechanical rotation is converted to an electrical signal which, in turn, drives the x-axis of an x-y recorder. The y-axis is powered from the sensor (photomultiplier) on the spectrometer. This procedure facilitates direct readout of spectra, thus eliminating the time consuming interpolation of strip chart records.

NOTE

During the course of this program it became apparent that certain additional evaluation procedures were required to understand fully the changes which take place in the SiC crystals during regrowth from solution. This applies particularly to the transition metal additives which were found to affect the electroluminescent properties quite markedly.

Accordingly, apparatus has been constructed. However, time did not permit the full use of these experimental tools. For sake of completeness, the following account is included which describes these apparatus in detail.

The first of these experiments is an infrared transmission spectrographic analysis. We have designed a special purpose optical chopping attachment which mounts in front of a single beam Perkin-Elmer Model 112 spectrometer and converts this instrument into a high resolution, dual beam spectrophotometer. A cam-operated switch, synchronized with the chopping mirror, is used to time-share the output of the electronics console. The two signals which result, one corresponding to each of the two identical but separate input optical paths, are then fed to the two inputs of the log amplifier (described in an earlier report) so that the chart recorder reads directly $\log I_2/I_1$, where I_1 is the intensity of transmission thru path 1, and I_2 is the intensity of transmission thru path 2.

Figure 7 is a schematic optical path diagram of the P. E. unit with and without the chopper attachment in place. Figure 8 is a block diagram of the electronics modifications required.

By using the spectrometer arrangement as indicated, it is possible to compare the changes in transmission produced by a TSM zone pass by inserting a sample of the starting seed in path 1 and the regrown crystal in path 2. The chart recorder then reads to 3 decades the ratio of I_2/I_1. If no changes were caused by passage of the zone, a reading of 1.0 is obtained. Where changes have occurred, a reading either greater than or less than unity is obtained. This technique eliminates the variability of the

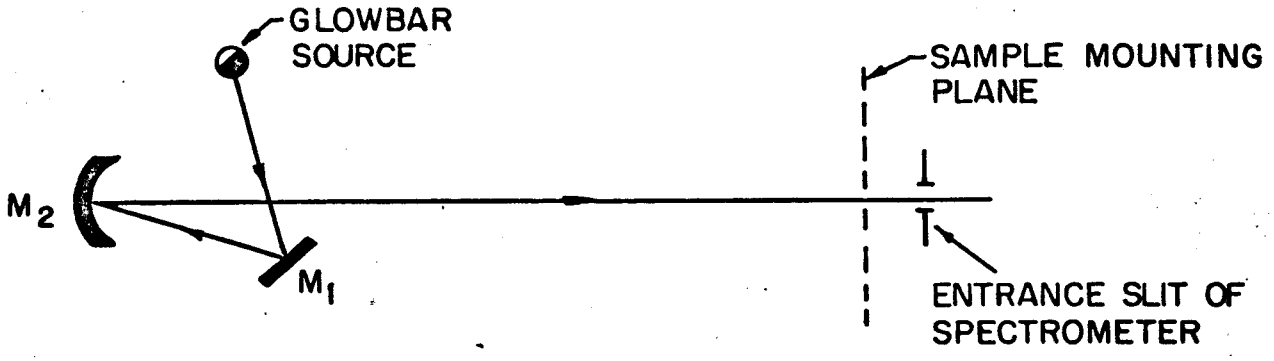

Fig. 7a P. E. 112 spectrometer source optics. Mirror M_1 is used to select which of the three sources provided (hydrogen arc, tungsten lamp, SiC glowbar) is to be imaged on slit by mirror M_2.

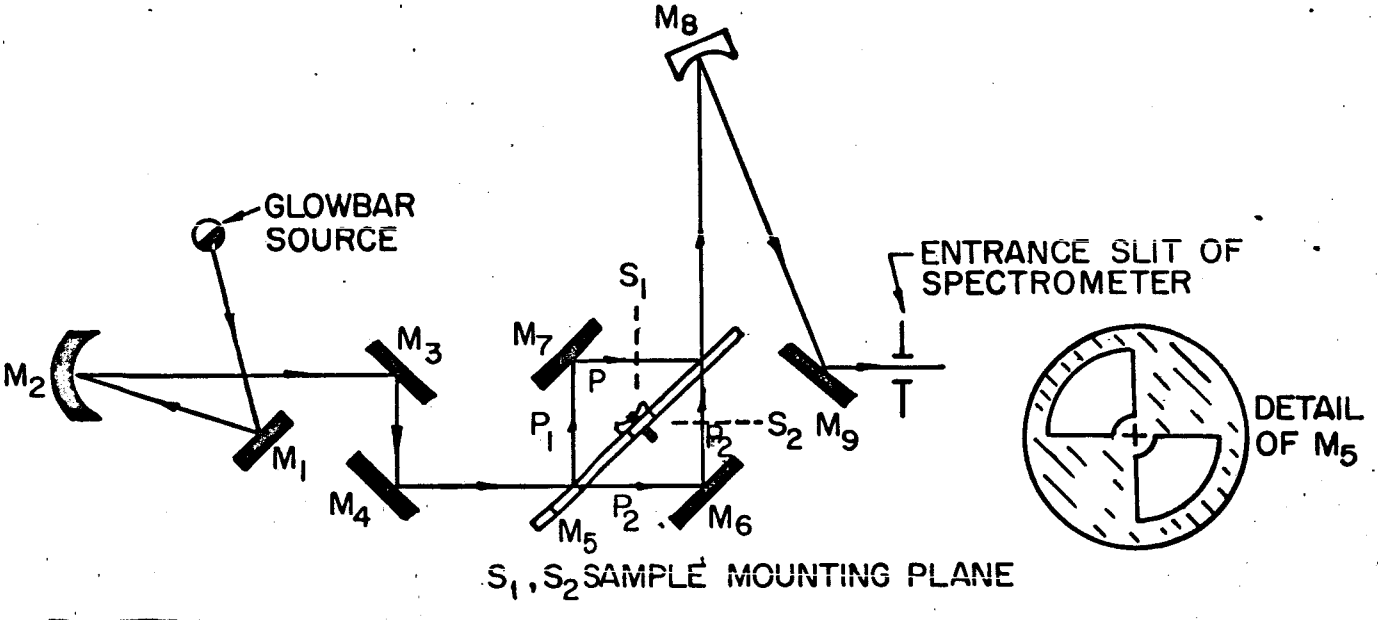

Fig. 7b P. E. 112 spectrometer source optics modified by optical attachment to provide two separate but equal optical paths, with two independent sample mounting planes. With mirror M_5 in the position where the mirrors are intercepting the beam, path P_1 is followed. Rotation of the mirror M_5 by 90^o puts the reflecting surfaces out of the interception region. The uninterrupted light beam passes through M_5 and follows path P_2, reflecting off M_6. Thus, as M_5 rotates, first P_1 and then P_2 is followed, with the light passing through sample S_1 and then S_2, this process repeating itself continuously.

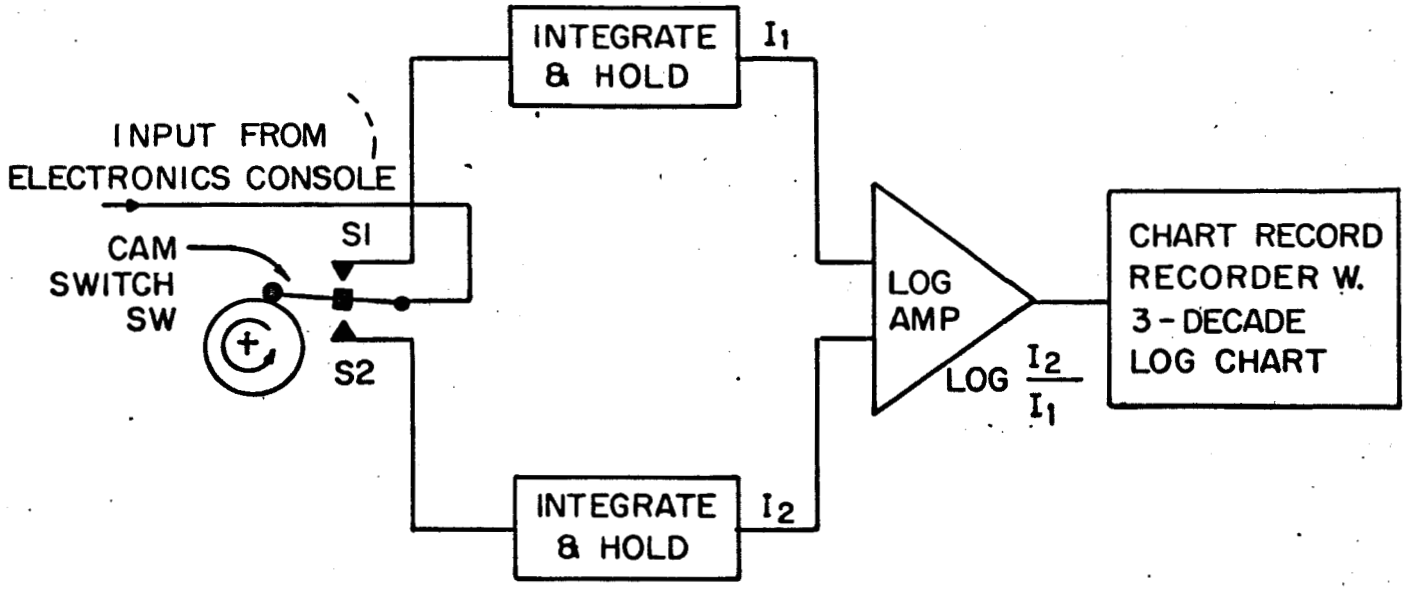

Fig. 8 Electronics required with optical apparatus of Fig. 7b Switch SW is a cam-driven switch operating in synchronization with mirror M_5 so that channel S_1 is connected to output I_1 when the light is following path P_1, and S_2 is connected to output I_2 when the light path P_2 is being followed. The integrate and hold circuits provide the necessary memory to allow display of the ratio by I_2/I_1. This ratio is formed in the log amplifier, described in an earlier report.

starting seeds from the measurement and shows only the changes produced by the growth conditions. Consistent appearance of a peak or valley when a known impurity is used will quickly locate an energy level of that impurity.

The infrared transmission experiment shows changes in optical absorption. It was also planned to determine optical emission, and an ultraviolet excitation system to optically simulate the crystals and record their re-emissions was set up. Information from this experiment, illustrated in Fig. 9, was to have been used to observe again changes caused by various dopants, and in addition, provide some information as to the emission process in SiC.

The final experiment to have been utilized is an alternating current Hall effect measurement which allows direct determination of the Hall effect in SiC without requiring either close geometrical control of the samples or perfect ohmic contacts. By the use of a modulation technique, the detector reads only the product of the magnetic field, B, and the current, I, flowing through the sample, and ignores completely effects due to sample thermoelectric voltages, offset voltages due to geometric misalignment of contacts, and nonlinear effects due to nonohmic contacts.

A schematic diagram of the system is shown in Fig. 10. A Halltron of InAs is embedded in a magnetic field of about 1 kg alternating at 60 cps. This field is produced by a pair of air core solenoid coils mounted in a Helmholtz configuration. The current driving the Halltron varies at the rate of 3 cps. The resulting Hall voltage produced by the Halltron therefore has frequency components at 3 cps, 57 cps, and 63 cps, and perhaps some also at 60 cps. This voltage is first amplified and then passed through

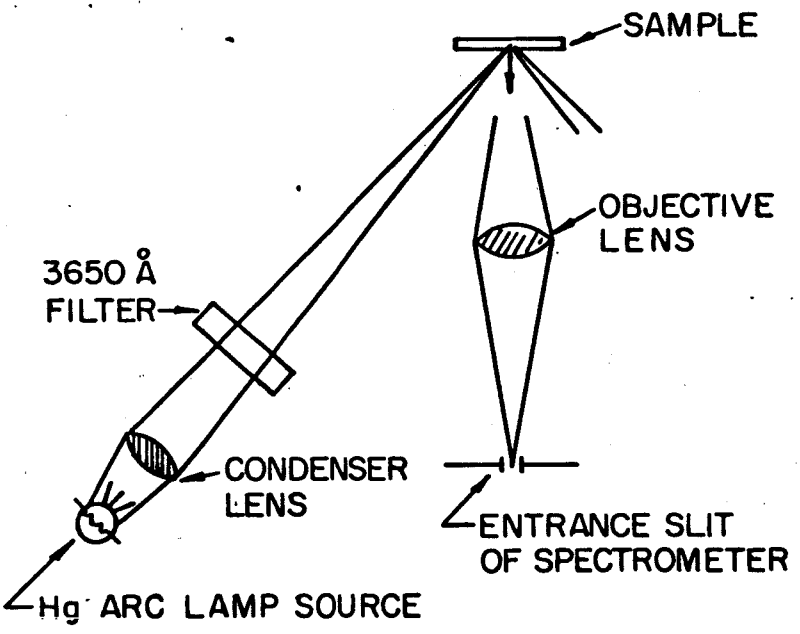

Fig. 9 Optical configuration of ultraviolet re-emission experiment. Spectrum will be examined in the visible region.

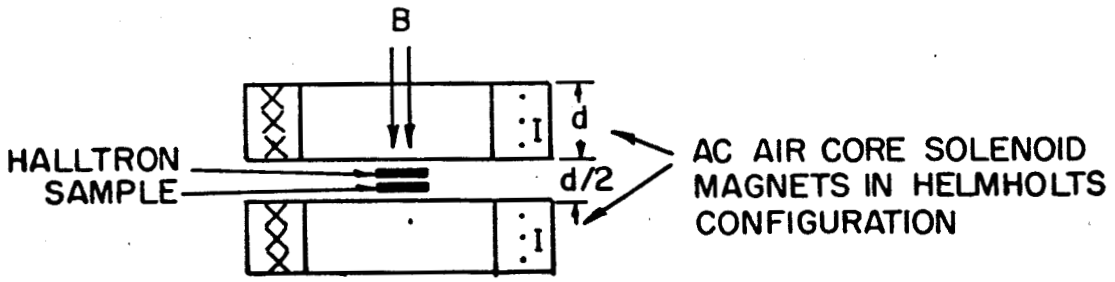

Fig. 10a Ac Hall effect measurement. Illustrating arrangement of Helmholtz magnets with sample and Halltron mounted parallel to each other at the center of symmetry.

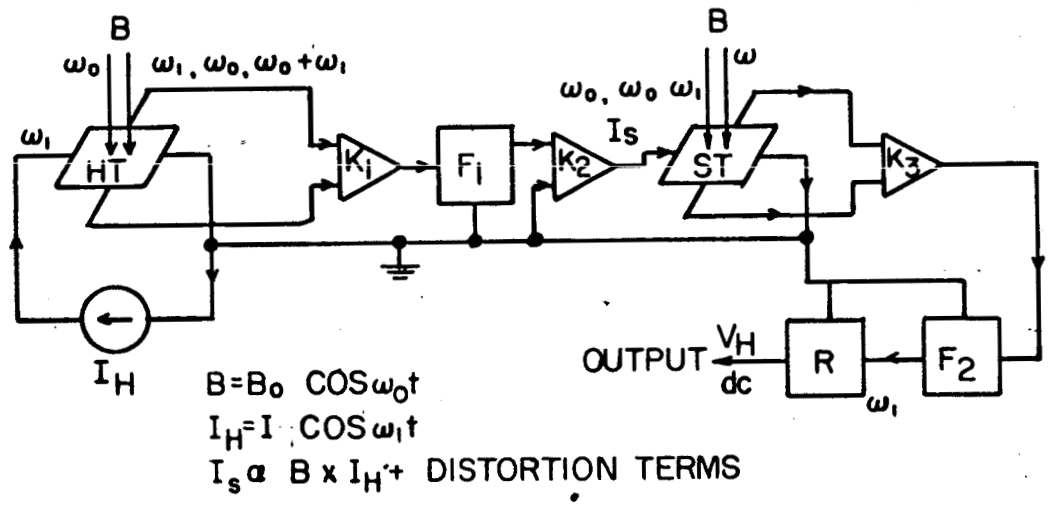

Fig. 10b Electronics system diagram. Halltron HT is driven by current source I_H and the magnetic field B. The output voltage of the Halltron is amplified by amplifier K_1 and then passed through the high pass filer F_1. At this point, the signal contains frequencies at ω_0 and at $\omega_0 \pm \omega_1$. This signal is fed into amplifier K_2, a voltage-to-current converter which drives the sample under test, ST. This sample is in the same magnetic field B as the Halltron. The output voltage of the sample is amplified by K_3 and then passed through the bandpass filter F_2 which only passes the frequency component ω_1. This component is the only one present which is unambiguously due to the Hall effect occurring in the sample. The signal is finally converted into a dc output by the precision rectifier R.

a high pass filter to remove the 3 cps component. The filtered signal then drives a current generator which supplies the current to the sample. The Hall voltage measured on the sample will contain the following frequency components: dc, 3 cps, 57 cps, 60 cps, 63 cps, 114 cps, 120 cps, 126 cps, etc.

Of these components, only the 3 cps component is due entirely to the true Hall effect; all other components result from defects in the sample preparation. Amplification and filtering of the sample Hall voltage to remove the 3 cps component (which is relatively easy to separate from the other components), and subsequent rectification of this signal results, finally, in a dc output proportional only to the product of B and I through the sample. This signal can be displayed directly on a recorder vs. temperature yielding a direct measure of the changes in carrier concentration in the sample vs. temperature. Comparison of this signal for a crystal before and after TSM zone passes can directly indicate the changes in electrical transport properties resulting from passage of the molten zone.

III. DEVICE TECHNOLOGY

A. Crystal Growth and Diode Construction

The basis of the preparation of p-n junction-bearing single crystals of α-SiC in this program has been the Travelling Solvent Method of Crystal Growth (TSM). This approach has been adequately documented, and further discourse does not appear necessary herein. However, for reasons of more efficient throughput and to alleviate certain problems associated with crystal growth from Cr-rich alloys containing other transitional elements, an evacuable crystal growth furnace was constructed some months ago.

Figure 11 is a schematic representation of the unit. The quartz vessel is double-walled (forming a water jacket) in the vicinity of the graphite rf susceptor upon which the specimens are placed. This provision enables a hard vacuum to be maintained within the system while the furnace is heated to the desired growth temperature (> 1600°C). Temperature control is obtained via the two-color, recording pyrometer which "sights" the upper surface of any one particular specimen. The output from the pyrometer is used to control the rf power from the induction unit. The system allows temperature control of $\pm$ 2°C at about 2000°C. This is, on any standard, very good temperature control.

Crystal growth can be made through either the p-type or n-type side. Generally, it is preferred to pass the molten zone through the n-type side since, in this case, the original doping levels are easier to maintain simply by the introduction of a small quantity of nitrogen into the furnace cavity.

NOTE

A very common characteristic of SiC crystals prepared by growth of p-type onto n-type (or vice versa) material is a thin, almost colorless region at the p-n junction. Simple interdiffusion of the Al (p-type) and N (n-type) impurities does not yield this effect. Since the extent of the colorless region varies with both solvent thickness and temperature of growth, we hypothesized that it resulted from the removal of both Al and N in the form of the compound AlN. Aluminum nitride is insoluble in SiC and would be contained in the liquid phase during growth. Such a process requires that, during the initial stage of growth (i.e. while the Cr is becoming saturated with SiC), dissolution from both sides occurs. Such is known to be the case.

To test the above idea, crystals were grown using an alloy of nominal composition Cr-20% wt SiC; the solvent is, therefore, virtually saturated with solute prior to heating. The outcome of

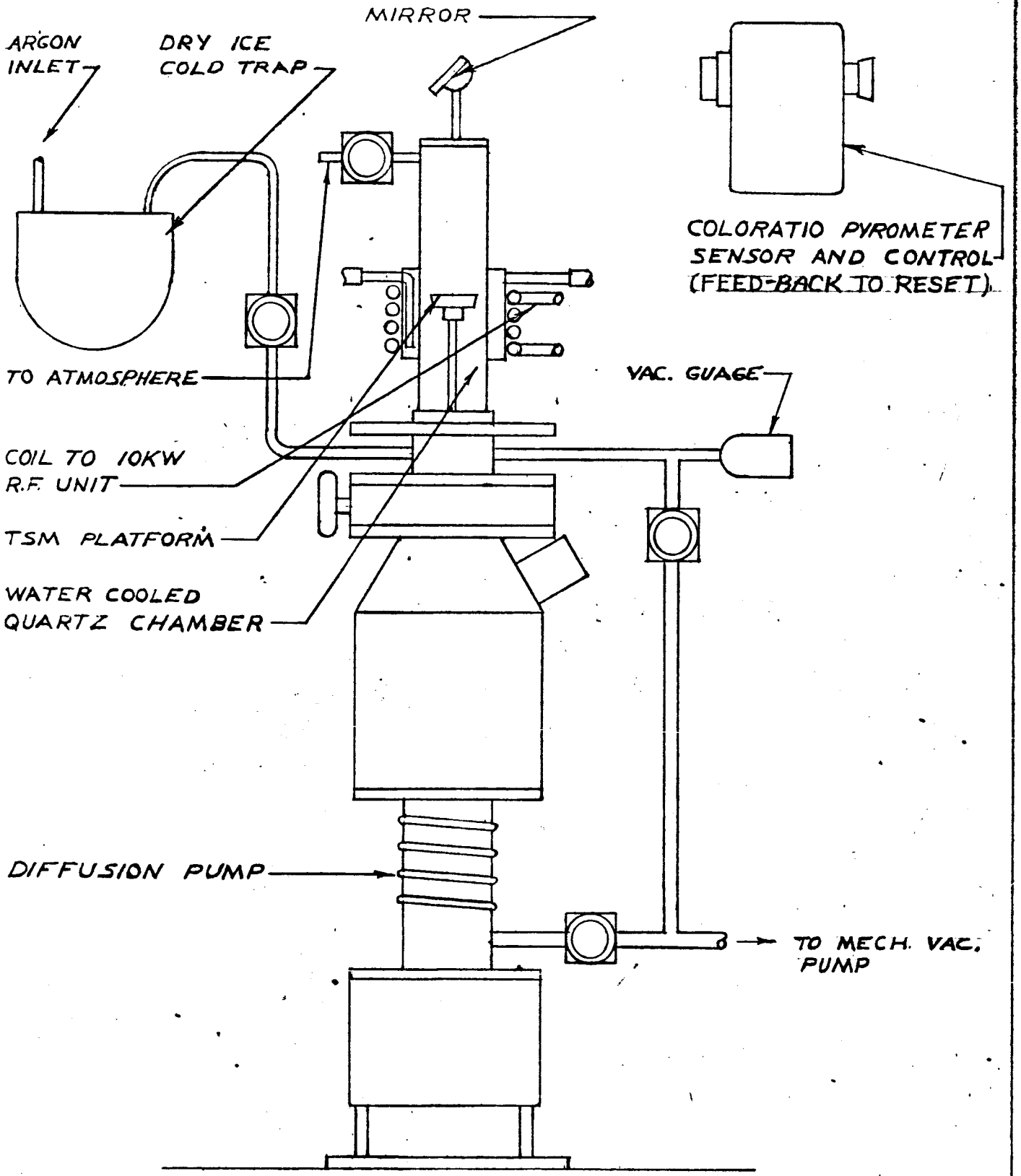

Fig. 11 Evacuable TSM crystal growth apparatus (schematic).

the experiment was quite straightforward. Working with pre-saturated Cr, absolutely no evidence of the clear region was obtained.

This result is very important from the device viewpoint, since the over-all resistance of our devices is obviously affected by inclusion of what is in fact a high resistivity region.

The majority of work on diode preparation has involved "doping" with transition elements. To this end, the solvent is a Cr-based alloy containing about 20% SiC (see foregoing note) plus up to 4 wt % of the desired element (e.g. Ti, Zr, Cu, Fe, Ni, Mn).

Following crystal growth (the process typically requires two hours), the crystal is cut into strips of 25 mil width. Because of the pronounced color differences the position of the junction may be readily determined by visual inspection. By a succession of lapping-inspection cycles, each side of the junction is reduced until the total thickness is 2-1/2 mil.

The next stage is that of providing ohmic contacts. These procedures are described in detail in section IIIB below.

Following contacting, the long sides of each strip are cleaned (i.e. the contact metal is removed) by cutting with a 5 mil-width diamond saw. The specimen is then cut into small blocks by cleaving with a razor blade. The resultant chips typically measure 12 mil x 7 mil x 2-1/2 mil (the total thickness of the contacts is only a few tenths of 1 mil).

It is important to note that α-SiC does not generally cleave along prismatic planes, i.e. normal to the plane of the p-n junction. However, in practice it is possible to affect quite good, flat fractures providing a very thin (i.e. a few mil) specimen is used. Subsequently, the small diode chips are soldered into heavy copper leaders (this facilitates good heat-sinking) using a standard Pb-Ag solder melting at 305°C. The top diode surface is contacted with a

5 x 15 mil silver tape which is also soldered with the same binary alloy. Figure 12 is a photograph of a completed α-SiC diode prepared in accordance with the foregoing description.

B. Contacting Techniques

We have examined and compared two different methods for making ohmic contacts to α-SiC diodes. The first of these involves the use of electroplated nickel followed by sintering and the simple "recipe" is as follows:

The 25 mil-width strip (cut from the as-grown crystal) is gripped in forceps and made the cathode in a standard sulphate plating bath. A very thin layer of nickel is thus deposited upon the slice. The nickel is then sintered into the surfaces of the SiC at the melting point of nickel. The cycle is then repeated and a final thin nickel plated layer applied, but without further sintering. This final plated layer facilitates soldering onto the copper header in the manner described in section IIIA above.

We have found the above method to be good for material of low resistivity, although the contacts exhibit linear I-V characteristics over only limited current ranges.

Accordingly, we have investigated alloys of Au-Ta which have been known for some time to provide good contacts to SiC. In the usual procedure small preforms of the alloy are melted directly onto the SiC surface. Such a technique is very time consuming and, in addition, difficult to control. It was therefore decided to investigate a different approach with Au-Ta. The following was ultimately found to be quite satisfactory.

1. Clean crystal chips in organic solvents using ultrasonic agitation
2. Lightly etch in hydrofluoric acid, wash, and dry
3. Sputter on a thin layer of tantalum - 5×10^{-2} mm Hg of argon for 2 hours, (750 volts, 0.5 amps)

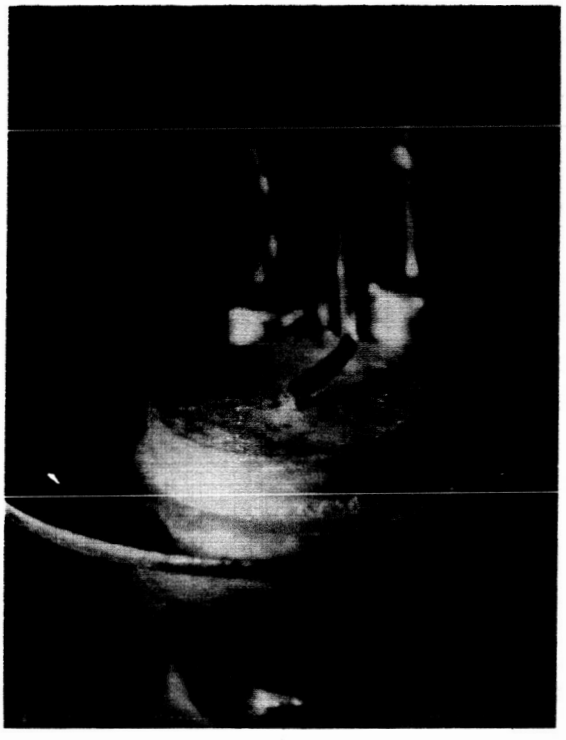

Fig. 12 Photograph of fully mounted TSM-grown α-SiC diode (X8).

4. Evaporate (in vacuum) a thin layer of gold
5. Evaporate a thin film of aluminum (for p-type material only)
6. Alloy the evaporated metals into SiC by heat treatment at 1350°C in an argon atmosphere
7. Evaporate a thin layer of Ni onto the alloyed surfaces
8. Sinter nickel into surface (this facilitates easier soldering to the header, etc.).

The above process has the inherent advantages of very precise control, particularly in the control of the quantity of metal applied, and also many samples may be loaded into a combination sputter/evaporation system and thereby treated simultaneously.

Using the contact evaluation procedures described in section II a comparison of the two contacting procedures have been made. Table II summarizes the data obtained.

The results show that the Au-Ta contacts are more uniform in behavior and yield, in this test, specific resistances one-half to one-fifth that of Ni contacts on material that is, in some cases, nearly 4 times more resistive. Taking into account the fact that approximate diode bulk series resistance subtracts 2 to 3 ohms from the total resistance, the effective contact resistances of the Au-Ta are even better by comparison.

Further evaluation of Au-Ta alloy contacts was made and a sample of the resultant data is shown in Tables III and IV. Figure 13 shows some results of experiments on which the effect of temperature upon the degree of non-linearity as a function of current density was determined.

TABLE II

Diode No.	Contact	V_f at 100 μa	V_f at 3 ma	V_f at 50 ma	V_f at 100 ma
127-3	Ni	.24	1.02	2.54	2.94 *
127-TA5	Au-Ta	.35	1.02	2.25	2.68
127-4	Ni	1.04	2.34	3.95	5.00
127-TA1	Au-Ta	1.27	2.35	3.15	3.56
127-5	Ni	2.12	2.62	5.25	6.57
127-TA2	Au-Ta	2.07	2.38	3.30	3.85

*Reading made at 80 ma.

TABLE III

Specific Contact Resistance of Evaporated
Au/Ta/Al Contacts to p-Type SiC

Sample No.	Sp. Contact Resistance OHM/CM^2 (25°C - 25 ma/cm^2)	Electrical Quality of Contact
1	1.0×10^{-2}	OHMIC
2	-	NON-OHMIC
3	1.3×10^{-2}	OHMIC
4	3.6×10^{-2}	OHMIC
5	0.6×10^{-2}	OHMIC
6	1.3×10^{-2}	OHMIC

TABLE IV

Non-Linearity of Au/Ta/Al Contacts

Sample No.	% Non-Linearity (25°C, 1 volt peak-to-peak signal)	Electrical Quality of Contact
1	0.024	OHMIC
2	6.60	NON-OHMIC
3	0.006	OHMIC
4	0.09	OHMIC
5	0.003	OHMIC
6	0.009	OHMIC
7	0.08	OHMIC
8	0.44	OHMIC
9	1.10	SLIGHTLY NON-OHMIC
10	0.006	OHMIC
11	0.5	OHMIC
12	0.45	OHMIC

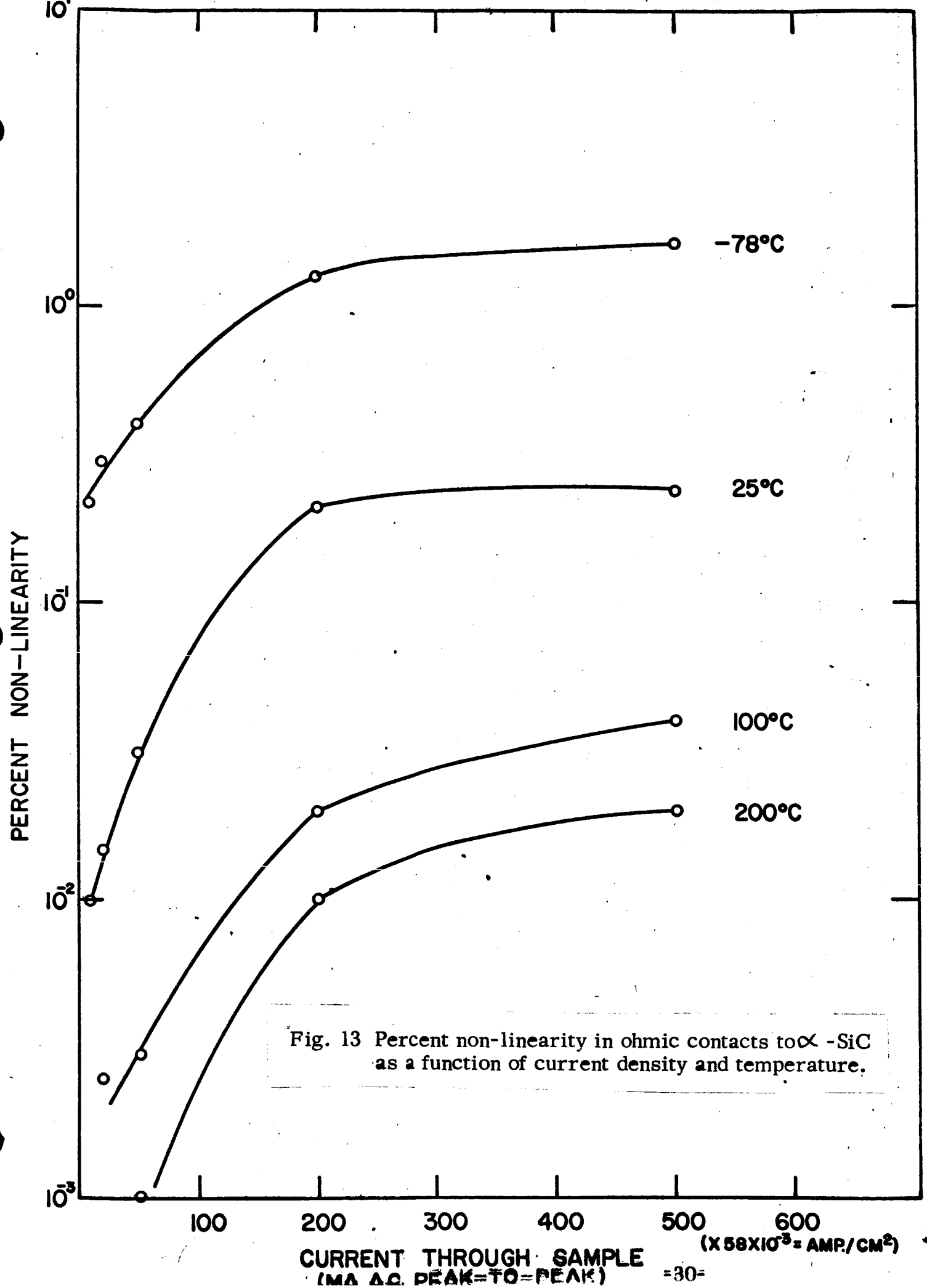

Fig. 13 Percent non-linearity in ohmic contacts to α-SiC as a function of current density and temperature.

IV. ELECTRO-OPTICAL PROPERTIES OF DIODES

Quite early in our investigations of the electroluminescent properties of α-SiC p-n junction diodes prepared by TSM, certain apparent requirements relating to the nature of the junctions emerged. These included:

1. A certain maximum junction width. This was determined from capacitance measurements at zero bias; and

2. A specific physical (crystallographic) structure of the junction-bearing region of the single crystal. This was found to take the form of a basal plane dislocation network.

In addition to the above, heavy doping on both sides of the junction is obviously beneficial in minimizing the total bulk resistance of the devices. Accordingly, continued attempts have been made to provide high doping levels during crystal growth experiments. In fact, by provision of a nitrogen atmosphere during growth through n-type material we have been able to maintain carrier concentrations in the range 10^{18} - 10^{19} · cm^{-3}. Table V illustrates data on some typical diodes, while in Table VI, additional data on some diodes are presented. Regarding items 1 and 2 above, we have reproduced these conditions on numerous occasions. The most important parameter in this context is the growth temperature. Low growth temperatures (< 1750°C - 1800°C) minimize interdiffusion (therefore junction width) across the junction. An upper limit of the junction width appears to be about 0.4 μ as determined from capacitance measurements. In addition, low growth temperatures provide for the basal plane dislocation network.

However, a significant conclusion reached following evaluation of very many diodes prepared under different conditions is that while the rectifying properties of the diodes can be understood in terms of these parameters, the electroluminescent properties cannot be explained by these alone.

TABLE V

α-SiC Diode Characteristic at 25°C

(Effect of Nitrogen Impurity Addition)

Diode No.	R_s (Ω)	C_o ($\mu\mu$f)	C/A (Pt/mil^2)	Carrier Conc/cm^3
TFR 15-3 **	> 232	464	2.1	4.3×10^{18}
15-2 **	> 535	305	1.3	9×10^{18}
TFR 17-2	447	228	.95	1.2×10^{18}
17-1	220	331	1.37	3×10^{18}
TFR 19-1 *	27.5	989	4.5	1.8×10^{19}
19-2 *	25	635	2.98	9×10^{18}
19-5 *	62	893	4.06	1.5×10^{19}
TFR 21-1 *	33	778	3.35	1.1×10^{19}
21-2 *	42.6	772	3.35	1.1×10^{19}
21-3 *	55	493	2.14	4.5×10^{18}
21-4 *	62	613	2.66	7×10^{18}
21-5 *	41	563	2.43	6×10^{18}

* Junction grown with nitrogen impurity addition.

** Junction grown with titanium impurity addition together with N_2.

TABLE VI

α-SiC Diode Characteristics - Figure of Merit

Diode No.	C_o ($\mu\mu$f)	C/A ($\mu\mu$f. mil^{-2})	Carrier Conc/cm^{-3}
TFR 38-2	712	2.58	6.8×10^{18}
TFR 38-1	748	2.7	7.0×10^{18}
TFR 37-4	1141	4.15	1.6×10^{19}
TFR 37-2	1573	5.8	2.9×10^{19}
TFR 37-3	1664	6.05	3.0×10^{19}
TFR 37-1	1785	6.5	3.5×10^{19}
TFR 35-5	710	2.2	5.2×10^{18}
TFR 35-4	655	2.04	4.5×10^{18}
TFR 35-3	508	1.57	2.8×10^{18}
TFR 35-2	445	1.39	2.25×10^{18}
TFR 35-1	107	.334	1.9×10^{17}
TFR 31-1	353	1.41	2.35×10^{18}
TFR 30-3	353	1.61	2.9×10^{18}
TFR 30-2	294	1.34	2.15×10^{18}
TFR 30-1	392	1.79	3.6×10^{18}
TFR 29-1	484	2.09	4.7×10^{18}
TFR 27-3	679	2.46	6.2×10^{18}
TFR 27-2	627	2.27	5.6×10^{18}
TFR 27-1	785	3.1	9.4×10^{18}
TFR 26-5	707	2.56	6.8×10^{18}
TFR 26-3	440	1.59	2.9×10^{18}
TFR 26-1	1142	4.1	1.6×10^{19}
TFR 25-3	886	3.66	1.3×10^{19}
TFR 25-2	990	4.06	1.5×10^{19}
TFR 25-1	620	2.58	7.0×10^{18}
TFR 24-5	310	1.04	1.4×10^{18}
TFR 24-4	107	.36	2.2×10^{17}
TFR 24-1	104	.35	2.0×10^{17}

In other words, while the foregoing may be necessary conditions for the attainment of a radiational recombination process exhibiting sufficient gain for ultimate laser action, they are definitely not sufficient conditions. The hypothesis proposed was that relatively deep levels are involved in the electroluminescent properties of indirect gap semiconductors. To this end, much of our effort has been directed towards the introduction of transition elements into α-SiC and to evaluating the electro-optical consequences thereof. (It is noteworthy that spectrographic analysis of SiC crystals from which high efficiency light output was observed previously revealed the presence of quite large quantities of transition metals).

General confirmation of the above hypothesis was initially obtained on diodes in which manganese was added, via the chromium solvent, during crystal growth. Figure 14 serves to illustrate the results in this instance.

It is clear that addition of the transition metal manganese results in a shift of the peak in the emitted radiation from the green towards the red. This result shows clearly that a specific impurity (level) can be pumped electrically in this semiconductor. Variations in the concentration of the major (nitrogen and aluminum) dopants does not yield this general effect.

Additions of the elements Fe, Ni, and Cu resulted in very poor devices, even in terms of the rectification characteristics. Accordingly, further work involving these was discontinued.

In all cases, so called "control-specimens" were prepared simultaneously with those to which the transition metal was added. In all other respects all junction-bearing crystals were prepared in an identical fashion as far as is possible with SiC. Major emphasis has been placed upon determination of the quantum efficiency and its variation with current density of the electro-luminescent process. The most promising results have been obtained with some of those

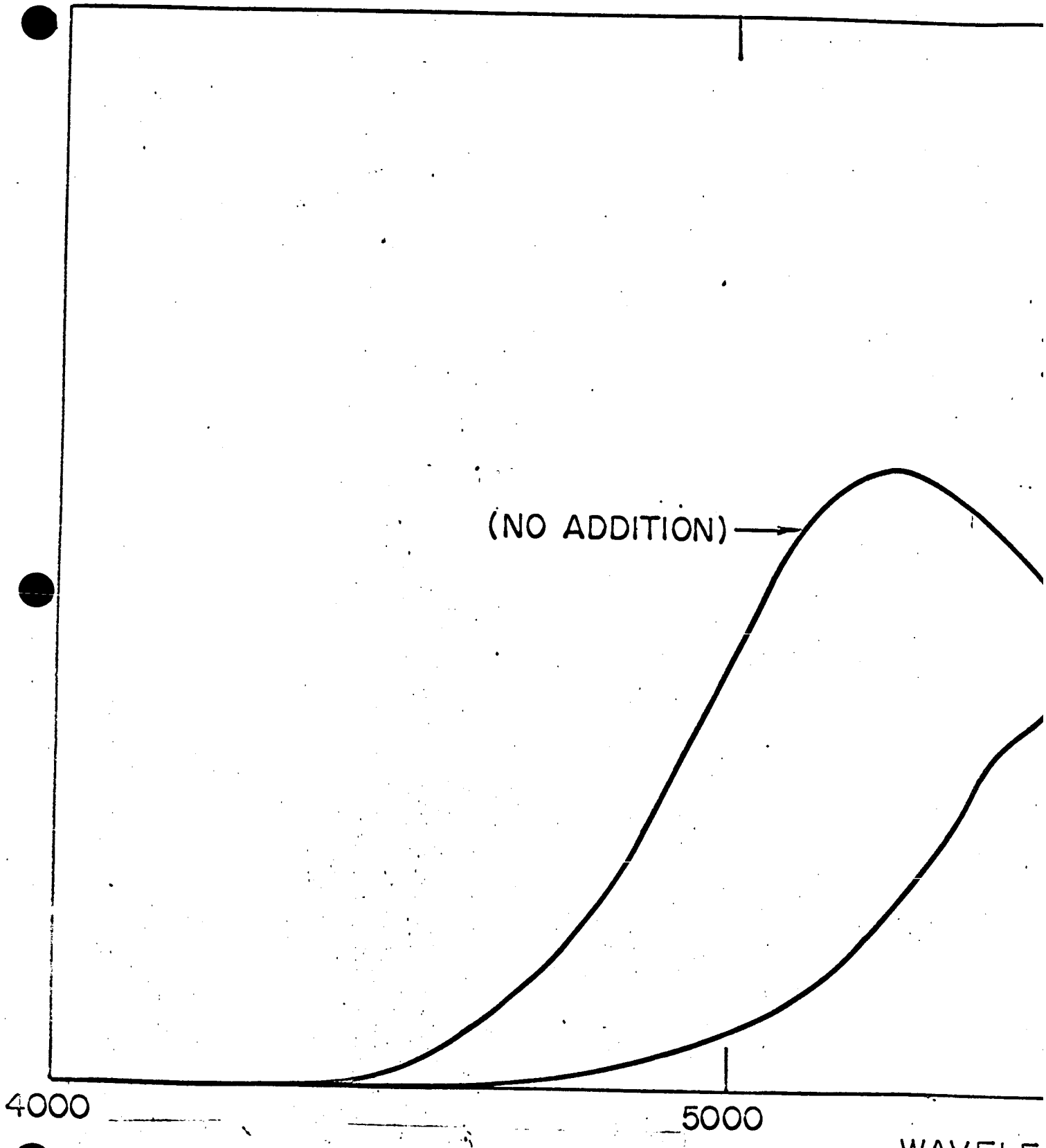

Fig. 14 Effect of Mn on the spectral distribution of α-SiC diodes under forward bias.

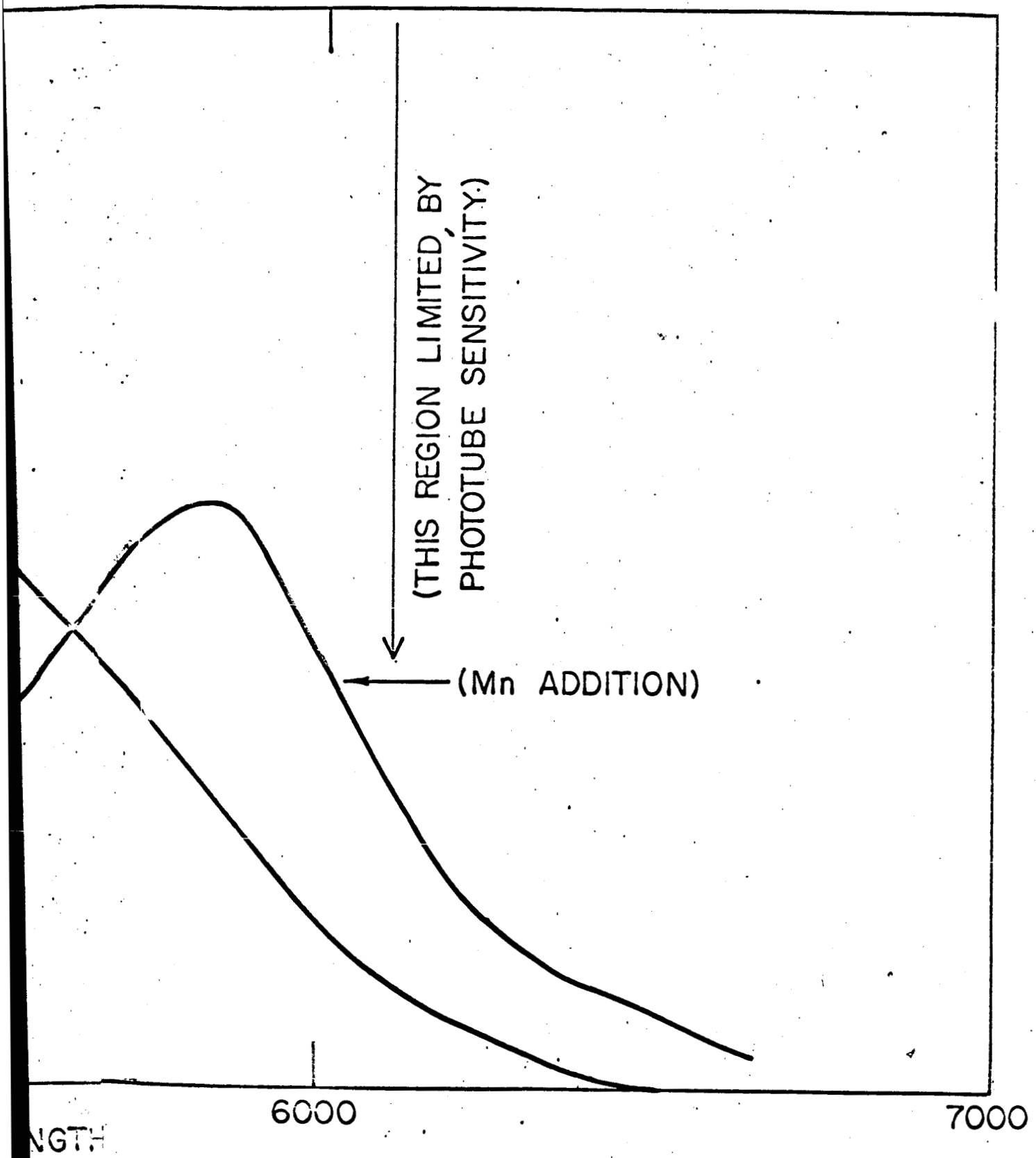
(THIS REGION LIMITED BY PHOTOTUBE SENSITIVITY)
(Mn ADDITION)
6000
7000
NGTH

2

diodes to which the elements titanium and zirconium were added via the chromium-rich solvent during crystal growth. (Alloys containing 2 wt % and 4 wt % of these two metals have been used).

Figure 15 summarizes the general trend observed and relates the light output power as a function of forward-bias current density. Since there was considerable scatter between the various diodes examined, the results are presented as bands rather than single lines.

The data from which Fig. 15 was constructed were obtained under forward-bias dc conditions of up to 500 amp/cm^{-2}. In Table VII some data relating quantum efficiency with current densities of up to greater than 10,000 amp/cm^{-2} are presented. These data were obtained under pulsed conditions using the photomultiplier detector system described previously.

TABLE VII

Variation of Quantum Efficiency of a Diode Grown from a Cr-2% Ti Alloy
(Room temperature measurements)

Current Density Amp. cm^{-2}	Quantum Efficiency %
500	8.6×10^{-5}
2,900	9.4×10^{-4}
5,800	1.58×10^{-3}
8,700	3.16×10^{-3}
11,600	6.3×10^{-3}

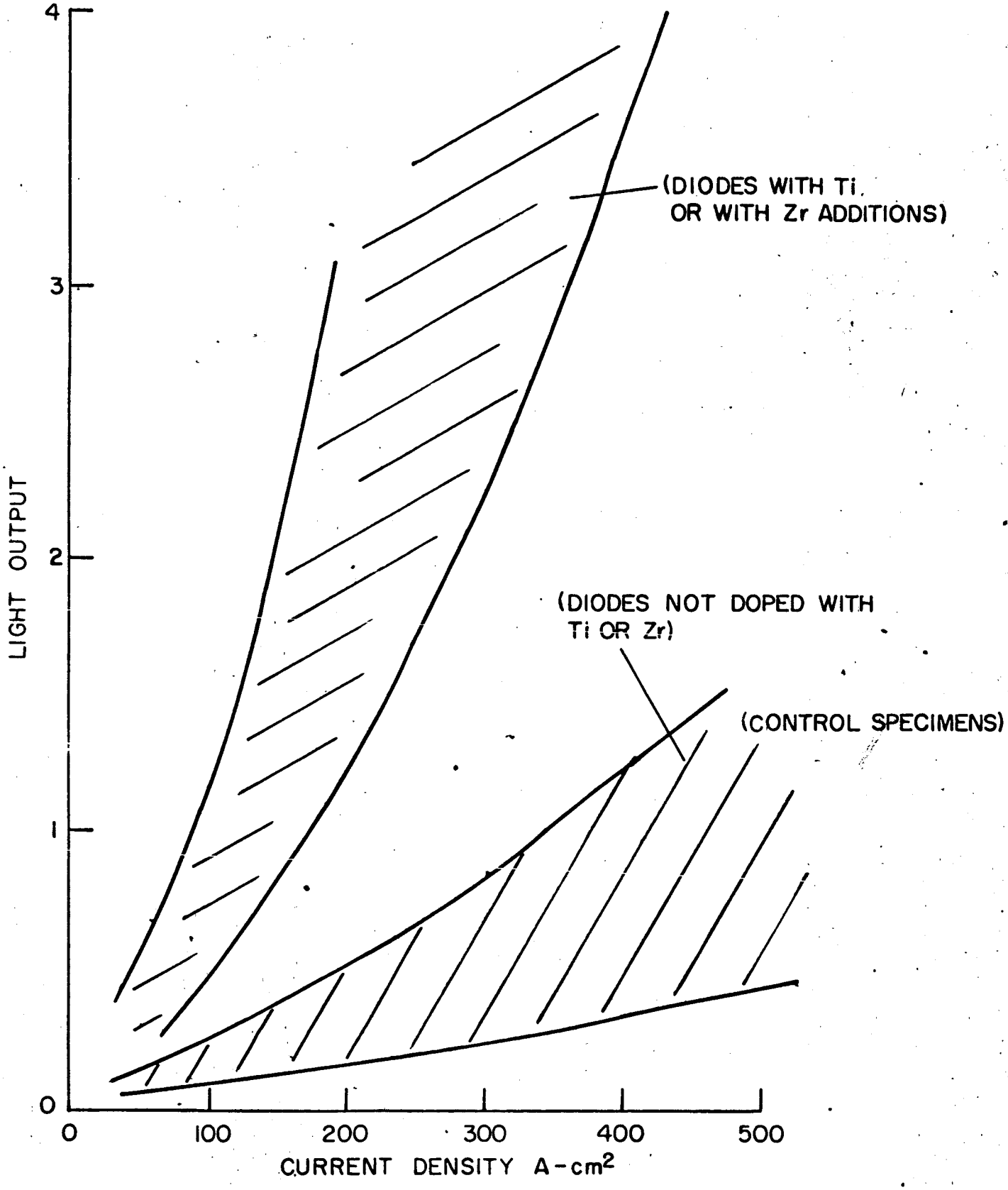

Fig. 15 Comparison of electroluminescence from α-SiC diodes with and without additions of Zr or Ti(room temperature).

The results (Fig. 15 and Table VI) obtained from Ti-and Zr-bearing diodes are, it is submitted, of considerable significance. Regrettably, device resistances have too frequently severely limited the current densities, even under pulsed conditions, to which we have been able to subject the diodes.

Finally, we have found no systematic trends relating the variation of quantum efficiency with temperature. This has been found to be the case, both at high and at low current densities. It appears that very pure SiC crystals, with accurately known impurity contents, will be required before the details of the temperature dependence of electroluminescence in α-SiC emerge.

V. CONCLUSIONS

1. Technology has been developed which enables the preparation of fully mounted, heat sunk diodes of α-SiC. A novel approach to contacting was developed. This technology is applicable to devices intended either for rectification or electroluminescent application.

2. It has been demonstrated that impurity levels (presumably deep) introduced from solution during crystal growth play a significant role in the details of the electroluminescent properties of SiC. Both the spectral distribution and the efficiency of the radiational process are affected.

Additions of Ti and Zr appear beneficial.

3. Attainment of high doping levels to minimize bulk resistances in α-SiC diodes is an acute problem. As we have demonstrated, however, it is not insurmountable.

4. A very systematic program of work is now required if the mechanisms of radiational recombination in α-SiC are to be appreciated. This is particularly relevant in view of the effects of certain transition metals. Until this is done little more progress is likely in this connection.